The Analysis of Short Signal Segments and its Application to Drive-By Bridge Inspections

Eugene J OBrien[#1], Jennifer Keenahan[*2]

[#]*The School of Civil Engineering, University College Dublin*
University College Dublin, Belfield, Dublin 4, Ireland
[*]*Arup Consulting Engineers, 50 Ringsend Road, Dublin 4, Ireland*

Abstract — *'Drive-By' damage detection is the concept of using sensors on a passing vehicle to detect damage in a bridge. At highway speeds, the vehicle spends a short amount of time on the bridge: it may not even go through a full oscillation, resulting in only a partial signal of the bridge motion being detected. Given that the spectral resolution of standard signal processing techniques depends on the length of data in the signal, they cannot be used to identify the bridge frequency accurately. In addition, the nonlinear and non-stationary nature of the vehicle-bridge interaction system poses challenges. An optimisation approach is proposed here as an alternative to standard signal processing techniques to overcome the challenges of short signals and the nonlinear nature of the drive-by system. Signal pollution due to the road profile is overcome using time-shifted bridge curvatures, a novel damage indicator.*

Keywords — *bridge, damage, optimisation, transforms, structural health monitoring, drive-by inspection*

I. INTRODUCTION

'Drive-by' bridge inspection [1] involves the instrumentation of a vehicle, rather than the bridge, in order to assess bridge condition. The approach has potential advantages in terms of reduced cost and ease of implementation. A limitation on the 'drive-by' concept to date has been the need for the vehicle to traverse the bridge at low speeds [2]–[5]. At highway speeds, the vehicle spends a short amount of time on the bridge. Therefore, the bridge may not even go through a full oscillation during the time that the vehicle is on it and as a result only a partial signal of the bridge motion is detected.

Most bridge damage detection methods use Fourier analysis as the principal signal-processing tool [6]–[9]. Joseph Fourier introduced the concept in the early 1800s [10], proposing that a signal could be formulated as a sum of weighted sinusoidal functions, which allows it to be analysed in terms of its frequency components. However, Fourier analysis has several shortcomings, in particular for the analysis of bridge dynamics. Firstly, it is unable to accurately represent non-periodic functions, due to the fact that it is derived on the assumption that the signal to be transformed is periodic and of infinite length [11]. Another deficiency is that Fourier analysis requires linearity, which proves a challenge as available data are frequently from systems that are nonlinear [12]. In addition, signals whose frequencies change with time, cannot be processed by Fourier analysis, due to that fact that the basis functions used (sine and cosine) go from negative infinity to positive infinity, and are not associated with a particular instant in time [13]. Lastly, the frequency components are obtained from an average over the whole length of the signal. This is a challenge when analysing signals of a non-stationary system [11], as measured signals produced by structural damage are of a non-stationary nature [6]. This is also a challenge for signals that are short in duration, such as the impulse response of cracked beams [14], or signals resulting from the 'drive-by' application [14], [15].

Based on Fourier analysis, the Short Time Fourier Transform (STFT) was later developed for processing non-stationary signals. Instead of analysing the entire signal at once, the STFT divides the signal into sections in time, using a window, and then analyses each of these sections separately with Fourier analysis [13]. The width of the window remains constant throughout the analysis and implicitly specifies the resolution of time and frequency information that will be obtained. The smaller the time duration of the window function, the better the time resolution and the poorer the frequency resolution [13]. A wide window results in a finer resolution of frequency but with worse time resolution. The STFT represents a compromise between time and frequency-based views of a signal. While the STFT represents an improvement on Fourier analysis for the processing of non-stationary signals, it is unable to accurately process very short signal segments. Cerda et al. [17] use an experimental model of a moving vehicle traversing a simply supported beam to examine the 'drive-by' concept, where changes in bridge condition are created by the addition of mass to the mid-span of the beam. Vertical acceleration signals from the vehicle are processed using the STFT. Results show that low vehicle speeds needed to accurately identify changes in bridge natural frequency.

The Wavelet Transform represents the next logical step in the development of signal processing methods: a windowing technique with variable size windows. Kim and Melham [14] describe wavelet analysis as a breaking up of a signal into shifted and scaled versions of a basis function known as the mother-wavelet,

resulting in variable sizes of the window function. Unlike Fourier analysis, where the basis function used is always sinusoidal, other basis functions, such as the Haar, Mexican hat, Coiflet, Daubechies and Morlet, can be selected according to the features of the signal [14]. The use of the Wavelet Transform for large crack detection was first proposed by Zhu and Law [18] where the deflection-time signal of a cracked beam subject to a constant moving load was analysed. Pakrashi et al. [19] numerically studied the comparative performance of different wavelet basis functions and windowing techniques in detecting damage, modelled in three different ways. Pakrashi et al. [20] also later conducted experiments and successfully monitored the evolution of a crack subject to vehicle-bridge interaction, using the Wavelet Transform. Later, Hester and González [21] further developed Zhu and Law's method for small cracks and compared the application of a number of different wavelet functions. They conclude that wavelets can be employed to identify damaged sections by using the response of a structure to a moving load, where the sensors are fitted to the bridge structure, and not the vehicle. However, the Wavelet Transform still suffers from the convolution of the signal with an a priori basis function [22] as available wavelet dictionaries are often not appropriate for analysing the nonlinear behaviour of many structural systems [23].

According to Huang et al. [12], the application of the Hilbert Transform has long been proposed as an advanced signal processing technique. The Hilbert transform is the convolution of the signal with the function $1/\pi t$, which emphasises its local properties. However, a drawback is that it requires a signal where the instantaneous frequency does not change with time, and intra-wave frequency modulation is typical of nonlinear systems. Cantero et al. [24] show how the natural frequencies of a bridge change with time, during the crossing of vehicles. A more recently developed method, the Hilbert-Huang Transform (HHT), has been proposed to overcome this challenge. The HHT uses Empirical Mode Decomposition (EMD) to decompose the signal into functions where the frequency does not change with time and then applied the Hilbert Transform. A further advantage of the method is that it has an a posterior, adaptive basis function, independent of the data, which is necessary for representing data that is nonlinear and non-stationary.

Authors that have used the HHT with EMD in a moving load context have found that the speed of the vehicle negatively impacts the success of damage detection. Bradley et al. [25] used EMD to detect a loss in stiffness in a 1D Finite Element beam structure subject to a moving load. They examined the effect of velocity of the moving load on the peak of the transformed signal, which indicated damage. Results showed that the greater the speed of the moving load, the smaller the damage peak and, the more difficult it

became to detect. Roveri et al. [26] applied the HHT to signals obtained from a beam modelled with an open crack, subjected to a moving load, to obtain the instantaneous frequency. It was found that, as the velocity of the load increased, the wave components became difficult to separate and thus the authors imposed a speed limit of 30 km h-1 on their work. This limitation of vehicle-bridge interaction in detecting the modal properties of a bridge cannot be overcome by increasing the scanning frequency of the sensors [16]. The underlying problem is that often the bridge had not undergone a full period of its fundamental frequency in the time it takes the vehicle to cross the bridge. Therefore, the only practical solution, if standard signal processing is to be used, is to decrease the velocity of the vehicle to capture more oscillations.

In this paper, an optimisation approach is proposed as an alternative to standard signal processing techniques to overcome the challenges of short signals, an example of which is the nonlinear system of 'drive-by' monitoring at highway speeds. Initially, one displacement sensor is considered on the vehicle as a proof of concept for the optimisation approach. The concept is then extended to two displacement sensors and the novel damage indicator of time-shifted curvatures is proposed as a means of overcoming the issue of the road profile. Vehicle motions are not considered.

II. OPTIMISATION AS AN ALTERNATIVE TO STANDARD SIGNAL PROCESSING TECHNIQUES

The concept of using an optimisation approach to determine the bridge frequency is based on minimising the sum of the squares of the differences between measured data and a theoretical expression, with frequency as the decision variable. Initially, the equation for a beam in free vibration is used to generate the measured data as this is comparable to the motion of a bridge exposed to the passing of a vehicle of much less mass:

$$u(x,t) = C\cos(\omega t - \alpha)\sin(\frac{nx\pi}{L}) \qquad (1)$$

where $u(x,t)$ is the displacement at position, x, and time, t, C is a constant representing the amplitude, ω is the frequency of vibration, α is a phase angle, n is the mode number and L is the length of the beam. The frequency of vibration, in rad s-1, is determined from:

$$\omega = (\frac{n\pi}{L})^2 k \qquad (2)$$

where k is square root of the beam stiffness divided by the beam mass. Taking values of $C = 1$, $\alpha = 0$, $k = 50$, $L = 10$ and $n = 1$, the frequency is analytically determined from (2) to be 4.9348 rad s-1. Beam displacements are determined using (1) for x varying in 0.1 m increments, and t varying in 0.005 s increments, corresponding to a speed of 20 m s-1. The value for $C = 1$ is chosen so that the displacements are normalised.

A. Single Sensor on the Vehicle Model with One Mode of Vibration

Initially, a single sensor is visualised on a vehicle model that can measure absolute vertical translation of the bridge. For the purpose of determining the data that this sensor would read, it was envisaged that the vehicle model would traverse the beam, but with no vehicle-bridge interaction. Fig. 1 illustrates the data that would be read by the sensor if it were present on the vehicle.
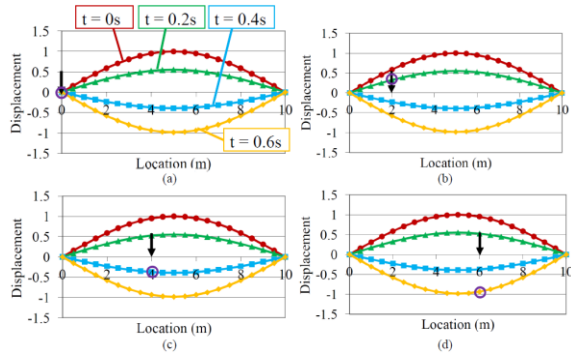

Fig.1 Bridge displacements read by the sensor on the vehicle model: (a) vehicle at start of bridge; (b) vehicle at 0.2L; (c) vehicle at 0.4L; (d) vehicle at 0.6L

In Fig. 1 (a), the sensor on the vehicle model reads the displacement at position $x = 0$ m at time $t = 0$. In Fig. 1 (b), the vehicle has moved 0.2L along the bridge. The displacement read by the sensor is from the second time curve (triangular data points) at $t = 0.2$, enclosed by the dark circle. In Fig. 1 (c), the vehicle has moved even further along the bridge and the displacement is read from the third time curve (square data points) at $t = 0.4$ and at position $x = 0.4L$. Scans of the bridge deflections are taken by the moving vehicle model at a spacing step of 0.1 m and a time step of 0.005 s, and are shown in Fig. 2
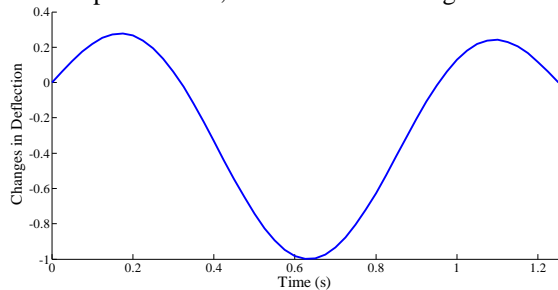

Fig. 2 Scan of the bridge deflections from the moving vehicle model for a single mode of vibration

TABLE I Actual and Inferred Frequencies for a Range of Damage Levels

k	Actual Frequency (rad s-1)	Frequency from optimisation (rad s-1)
50	4.9348	4.9348
49	4.8361	4.8361
48	4.7374	4.7374
47	4.6387	4.6387
46	4.5400	4.5400

An optimisation approach, which seeks to minimise the difference between measured data and a theoretical expression is used. The stream of displacements in Fig. 2 is taken as the measured data and (2) as the theoretical expression. The optimisation approach correctly determines the unknown bridge frequency in (1) to be 4.9348 rad s-1. Global damage is simulated as a change in the k parameter of (2). The actual frequencies for each damage level are determined analytically from (2). These frequencies, along with those determined by the optimisation approach, are presented in Table II and show excellent agreement with one another.

Fig. 3 illustrates the scanned bridge deflections from the moving vehicle model for different damage levels. There is a clear distinction between the curves, even for small changes in damage.
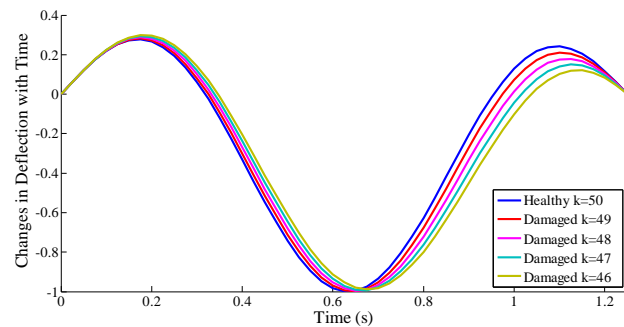

Fig. 3 Bridge deflections from the vehicle model for different levels of damage for a single mode of vibration

B. Single Sensor on the Vehicle Model with Two Modes of Vibration

The inclusion of a second mode of vibration results in a more complex expression for the displacement of the beam in free vibration, as in (3).

$$u(x,t)=C_1 \cos(\omega_1 t - \alpha_1)\sin(\frac{1x\pi}{L}) + C_2 \cos(\omega_2 t - \alpha_2)\sin(\frac{2x\pi}{L}) \quad (3)$$

where C_1 and C_2 represent the amplitudes of the first and second mode respectively, ω_1 and ω_2 are the frequencies and α_1 and α_2 are the phase angles. Using the parameter values of Table II, Fig. 4 gives the deformed shape of the bridge at a range of points in time. As before, the value of $C_1 = 1$ is chosen such that the mode one displacements are normalised, and the amplitude of mode two is taken to be one tenth of the amplitude of mode one.

TABLE II Parameter Values for Two Modes of Vibration

Parameter	Mode 1	Mode 2
C	1	0.1
α	0	0.7854
n	1	2
k	50	50

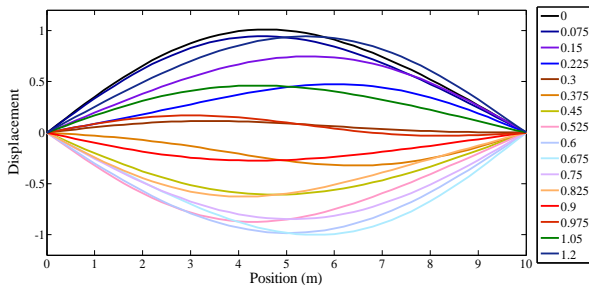| *L*	10	10	46	4.5400	18.16	1.00	0.10	0.7854

Fig. 4 Beam displacements for a beam in free vibration for the first and second mode

As before, a vehicle containing one sensor is considered to be traversing the beam at a speed of 20 m s-1 and scanning deflections every 0.005 s. Global damage is again simulated as a change in the *k* parameter of (2). Fig. 5 illustrates a scan of the bridge deflections from the vehicle for different levels of damage.
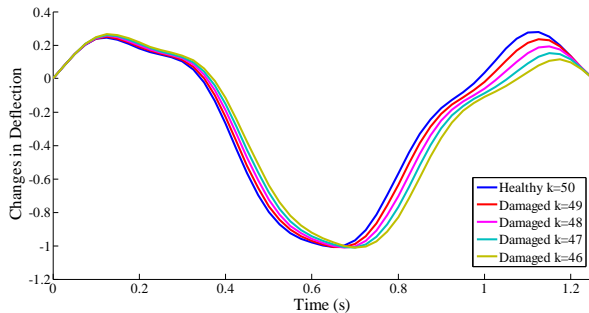

Fig. 5 Bridge deflections from the moving vehicle for different levels of damage for the first and second mode of vibration

It clearly illustrates that damage can be detected from a scan of bridge deflections read by a sensor on the vehicle model. A similar optimisation approach is used in this example where there are now five unknown variables; two frequencies, two amplitudes and the difference in phase angle between the modes. It is assumed here that the phase angle of the first mode is zero. The variables, correctly determined from the optimisation procedure, are given in the Table III and exactly match the actual values in the number of significant digits shown.

TABLE III INFERRED FREQUENCIES, AMPLITUDES AND PHASE DIFFERENCE FOR A RANGE OF DAMAGE LEVELS

k	ω_1 (rad s-1)	ω_2 (rad s-1)	C_1	C_2	Φ Diff (rad)
50	4.9348	19.73	1.00	0.10	0.7854
49	4.8361	19.34	1.00	0.10	0.7854
48	4.7374	18.94	1.00	0.10	0.7854
47	4.6387	18.55	1.00	0.10	0.7854

To gain an understanding on the conditioning of the system, a plot of the contours of the objective function (considering only the two frequencies as variables) is shown in Fig. 6, where the objective function is the sum of the squares of the differences between measured and theoretical data.
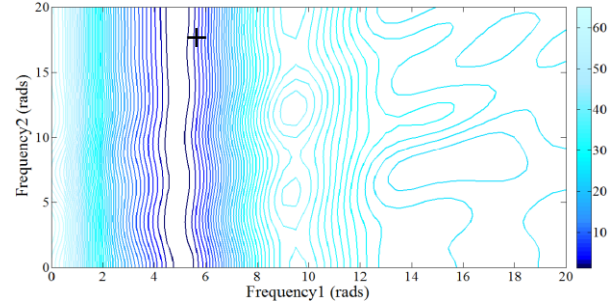

Fig. 6: Contours of the objective function (undamaged, k = 50)

The figure shows that the optimisation approach can find the global minimum in the range of frequencies from 0 to 20 rad s-1. The minimum is indicated in the figure by the black cross. The objective function is highly sensitive to the first natural frequency but insensitive to the second. However, it should be noted that it is the frequency of the first mode that will be used for damage detection and so the accuracy of the inferred second natural frequency is unimportant.

III. TIME-SHIFTED CURVATURES TO REMOVE THE INFLUENCE OF ROAD PROFILE

Often, the variations in road profile height are greater than the bridge deflections and thus the road profile masks the bridge motion. Much of the research to date in the field of drive-by damage detection has failed to comprehensively allow for the vehicle travelling at highways speeds and the presence of a road profile. McGetrick et al. [27] use numerical simulations to investigate the influence of a road profile on the feasibility of using an instrumented quarter-car to detect bridge natural frequencies. Results indicate that the approach works well in the absence of a road profile. However, when an ISO Class 'A' [28] road profile is included in simulations, the bridge frequencies are only detected for speeds up to 5 m s-1. The inclusion of road surface roughness in numerical simulations excites the vehicle to greater amplitudes than the bridge does and poses challenges in identifying bridge frequencies [29]. Fortunately, signal pollution due to the road profile can be overcome using time-shifted bridge curvatures. This is a unique type of curvature, with the first derivative of translation found with respect to position, and the second derivative found with respect to time:

$$\kappa = (SensorA - SensorB)_{t1} - (SensorA - SensorB)_{t2} \qquad (4)$$

where the speed is such that Sensor B at time t_2 reaches the same point that Sensor A was at time t_1. It follows that the data recorded by the first sensor, and the data recorded by the second sensor at a time lag corresponding to the axle-gap, both contain the same road profile heights. Thus, the process has the effect of removing the road profile heights from the time-shifted curvatures. These curvatures, along with the optimisation procedure described in Section II, are now proposed as an alternative to standard signal processing techniques, in the 'drive-by' concept, as the most comprehensive approach to date.

It is envisaged that a vehicle model with two sensors, here spaced at 2 m, will traverse the beam at a speed of 20 m s-1. Fig. 7 illustrates the process for a beam vibrating at the first mode only.
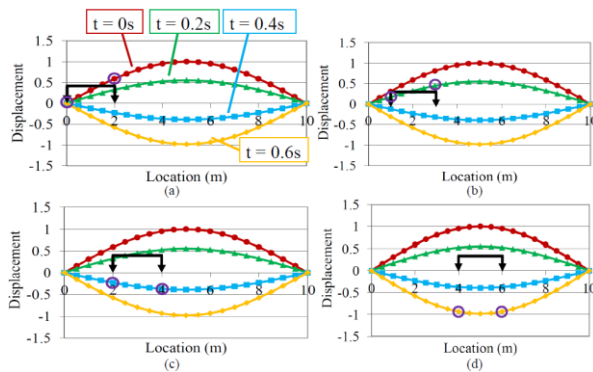

Fig. 7: Illustration of the data read by the two sensors (circles indicated deflection measurements) (a) t = 0; (b) t = 0.2; (c) t = 0.4; (d) t = 0.6

IV. THEORETICAL EXPRESSION FOR TIME-SHIFTED CURVATURES USING PHASOR ANALYSIS

Using the optimisation approach of seeking the minimum squared difference between measured data and a theoretical expression, (1) is now used to develop a theoretical expression for the time-shifted curvature. The displacement measured by the first vehicle sensor is:

$$u(x_1, t_1) = C \cos(\omega t_1 - \alpha) \sin\left(\frac{n x_1 \pi}{L}\right) \qquad (5)$$

where $u(x_1, t_1)$ is the displacement at position x_1 and time t_1. The displacement read by the second sensor at the same instant in time is:

$$u(x_1 + d, t_1) = C \cos(\omega t_1 - \alpha) \sin\left(\frac{n(x_1 + d)\pi}{L}\right) \qquad (6)$$

where d is the axle spacing. The difference between (5) and (6) is the distance-slope, simplified here using trigonometric manipulation:

$$\theta(t_1) = -\frac{C}{2}\left[\sin\left(\omega t_1 - \alpha + \frac{n x_1 \pi}{L}\right) - \sin\left(\omega t_1 - \alpha - \frac{n x_1 \pi}{L}\right)\right] + \frac{C}{2}\left[\sin\left(\omega t_1 - \alpha + \frac{n(x_1 + d)\pi}{L}\right) - \sin\left(\omega t_1 - \alpha - \frac{n(x_1 + d)\pi}{L}\right)\right] \qquad (7)$$

The time shifted curvature, κ, is the difference between distance-slopes at time t_1 and t_2, expressed in

(8). In (9) and (10) the implicit relationships between x_1, x_2, t_1, t_2 and d is provided.

For the purposes of optimisation, it is useful to re-write this expression as one sine wave rather than the sum of eight sine waves. This involves rewriting (11) as a vector whose magnitude is the signal amplitude and direction is the signal phase (12).

$$\left\{ \frac{C}{2}\left[\sin\left(\omega t_1 - \alpha + \frac{n(x_1 + d)\pi}{L}\right) - \sin\left(\omega t_1 - \alpha - \frac{n(x_1 + d)\pi}{L}\right)\right] \right.$$
$$\left. -\frac{C}{2}\left[\sin\left(\omega t_1 - \alpha + \frac{n x_1 \pi}{L}\right) - \sin\left(\omega t_1 - \alpha - \frac{n x_1 \pi}{L}\right)\right]\right\} -$$
$$\left\{ \frac{C}{2}\left[\sin\left(\omega t_2 - \alpha + \frac{n(x_2 + d)\pi}{L}\right) - \sin\left(\omega t_2 - \alpha - \frac{n(x_2 + d)\pi}{L}\right)\right] \right.$$
$$\left. -\frac{C}{2}\left[\sin\left(\omega t_2 - \alpha + \frac{n x_2 \pi}{L}\right) - \sin\left(\omega t_1 - \alpha - \frac{n x_2 \pi}{L}\right)\right]\right\} \qquad (8)$$

$$x_2 = x_1 + d \qquad (9)$$

$$\frac{x_1}{t_1} = \frac{x_2}{t_2} \qquad (10)$$

$$A \sin(\omega t + \phi) \qquad (11)$$

$$a + ib \qquad (12)$$

In (12) a is the real component of the vector, b is the imaginary component and i is the square root of negative 1. The amplitude and phase can be found from (13) and (14).

$$A = \sqrt{a^2 + b^2} \qquad (13)$$

$$\phi = \tan^{-1} \frac{b}{a} \qquad (14)$$

As all eight terms in (8) relate to the same frequency, they can be combined using phasor analysis and vector addition. The first term of (8), for example, in vector form, is given by Eq. (12) with:

$$\frac{C}{2} = \sqrt{a^2 + b^2} \qquad (15)$$

$$\frac{n(x_{r-d} + d)\pi}{L} - \alpha = \tan^{-1} \frac{b}{a} \qquad (16)$$

$$a = \cos\left(\frac{n(x_{r-d} + d)\pi}{L} - \alpha\right) \qquad (17)$$

$$b = \sin\left(\frac{n(x_{r-d} + d)\pi}{L} - \alpha\right) \qquad (18)$$

The Phasor representations of all eight terms are found in this way and are presented in Table IV.

It should be noted that the first four Phasors occur at one instant in time, and the second four at a later time (19).

$$\kappa = \kappa_1(t_1) + \kappa_2(t_2) \qquad (19)$$

Combining the first four expressions all associated with the same moment in time, gives:

$$\kappa_1(t_1) = 2C\cos\left(\frac{2nx_{r-d}\pi + nd\pi}{2L} - 2\alpha\right)\sin\left(\frac{nd\pi}{2L}\right) \quad (20)$$

Similarly, combining the remaining expressions associated with the other moment in time gives:

$$\kappa_2(t_2) = 2C\cos\left(\frac{2nx_r\pi + nd\pi}{2L} - 2\alpha\right)\sin\left(\frac{nd\pi}{2L}\right) \quad (21)$$

The addition of $\kappa_1(t_1)$ from $\kappa_2(t_2)$ is complicated by the fact that they occur at different times. By converting the time between the Phasors to an angle (based on the constant frequency property), a phase shift can be calculated between the two phasors. The phase angle β between the two phasors is found from (22).

$$\beta = \omega(t_2 - t_1) \quad (22)$$

This phase angle can be placed into the phase of one of the Phasors. The vectors can then be split into their orthogonal components and added, resulting in a single Phasor representing the time-shifted curvature.

TABLE IV PHASOR REPRESENTATION OF ALL EIGHT TERMS IN THE CURVATURE EXPRESSION

T	Phasor
1	$\frac{C}{2}\cos\left(\frac{n(x_{r-d}+d)\pi}{L} - \alpha\right) + i\frac{C}{2}\sin\left(\frac{n(x_{r-d}+d)\pi}{L} - \alpha\right)$
2	$\frac{C}{2}\cos\left(\frac{n(x_{r-d}+d)\pi}{L} - \alpha\right) - i\frac{C}{2}\sin\left(\frac{n(x_{r-d}+d)\pi}{L} - \alpha\right)$
3	$\frac{C}{2}\cos\left(\frac{n(x_{r-d})\pi}{L} - \alpha\right) + i\frac{C}{2}\sin\left(\frac{n(x_{r-d})\pi}{L} - \alpha\right)$
4	$\frac{C}{2}\cos\left(\frac{n(x_{r-d})\pi}{L} - \alpha\right) - i\frac{C}{2}\sin\left(\frac{n(x_{r-d})\pi}{L} - \alpha\right)$
5	$-\frac{C}{2}\cos\left(\frac{n(x_r+d)\pi}{L} - \alpha\right) - i\frac{C}{2}\sin\left(\frac{n(x_r+d)\pi}{L} - \alpha\right)$
6	$-\frac{C}{2}\cos\left(\frac{n(x_r+d)\pi}{L} - \alpha\right) + i\frac{C}{2}\sin\left(\frac{n(x_r+d)\pi}{L} - \alpha\right)$
7	$-\frac{C}{2}\cos\left(\frac{n(x_r)\pi}{L} - \alpha\right) - i\frac{C}{2}\sin\left(\frac{n(x_r)\pi}{L} - \alpha\right)$
8	$-\frac{C}{2}\cos\left(\frac{n(x_r)\pi}{L} - \alpha\right) + i\frac{C}{2}\sin\left(\frac{n(x_r)\pi}{L} - \alpha\right)$

This Phasor, by the inverse of the process described above, is then converted back to a sine wave of the form:

$$A\sin(\omega t_{r-d} + \tan^{-1}\phi) \quad (23)$$

where t_{r-d} is the initial time step of the first sensor, A is the amplitude, given in (24), and ϕ is the phase angle, given in (25).

$$A = \left[\left(\tan(\beta)\sqrt{\frac{\left(2C\cos\left(\frac{2nt_r\pi + nd\pi}{2L} - 2\alpha\right)\sin\left(\frac{nd\pi}{2L}\right)\right)^2}{(\tan\beta)^2 + 1}}\right)^2 + \left(2C\cos\left(\frac{2nt_r\pi + nd\pi}{2L} - 2\alpha\right)\sin\left(\frac{nd\pi}{2L}\right) - \sqrt{\frac{\left(2C\cos\left(\frac{2nt_r\pi + nd\pi}{2L} - 2\alpha\right)\sin\left(\frac{nd\pi}{2L}\right)\right)^2}{(\tan\beta)^2 + 1}}\right)^2\right]^{\frac{1}{2}} \quad (24)$$

$$\phi = \left(2C\cos\left(\frac{2nt_r\pi + nd\pi}{2L} - 2\alpha\right)\sin\left(\frac{nd\pi}{2L}\right) - \sqrt{\frac{\left(2C\cos\left(\frac{2nt_r\pi + nd\pi}{2L} - 2\alpha\right)\sin\left(\frac{nd\pi}{2L}\right)\right)^2}{(\tan\beta)^2 + 1}}\right) \div \tan(\beta)\sqrt{\frac{\left(2C\cos\left(\frac{2nt_r\pi + nd\pi}{2L} - 2\alpha\right)\sin\left(\frac{nd\pi}{2L}\right)\right)^2}{(\tan\beta)^2 + 1}} \quad (25)$$

This theoretical expression for time-shifted curvature can now be used in the optimisation approach.

V. FINDING TIME-SHIFTED CURVATURES IN THE DRIVE –BY CONCEPT

The beam displacements generated in Section II are used again here. Distance-slopes are calculated by subtracting the displacement readings from the second sensor of the displacement readings of the first sensor at each instant in time. These distance-slopes are presented in Fig. 8.
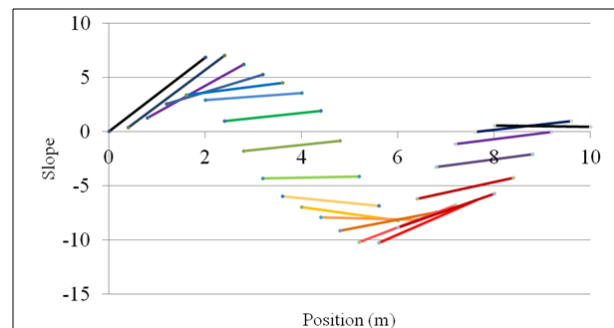

Fig. 8: Distance-slopes determined from the displacements recorded by the sensors

Taking position $x = 4$ m as an example, the distance-slope recorded at the second time interval (enclosed in the lower circle) is subtracted from the

distance-slope recorded at the first time interval (enclosed in the upper circle). The result is a time-shifted curvature that has allowed for the time-gap between the axles and has effectively removed the road profile heights. The variation in time-shifted curvature with time can be seen in Fig. 9.
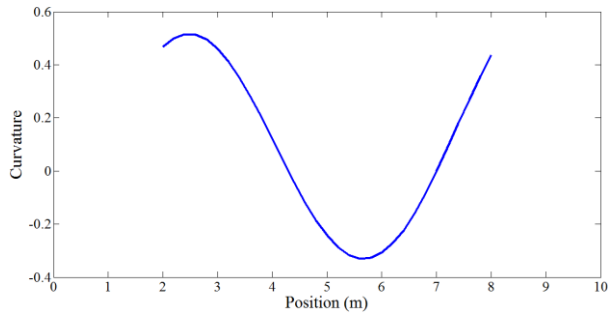

Fig. 9: Time-shifted curvatures for the first mode of vibration

Optimisation seeking to minimise the difference between the theoretical expression described in (23) (with the decision variable of frequency) and the measured data presented in Fig. 9, correctly determines the bridge frequency to be 4.9348 rad s-1.

Five different levels of damage are now simulated and Fig. 10 illustrates how the time-shifted curvature is influenced by damage, here simulated as a change in the beam stiffness parameter.

The actual frequencies of each damage level are analytically determined from (2). These frequencies, along with those determined by the optimisation approach, are presented in Table V.
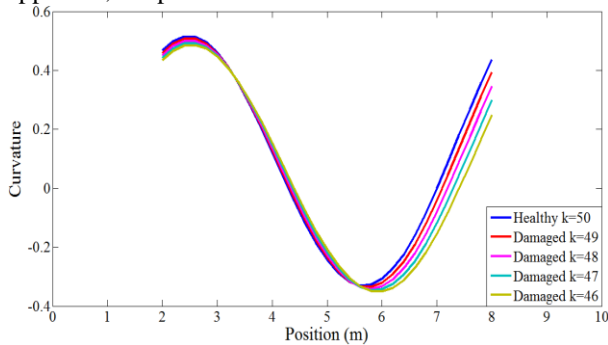

Fig. 10: Time-shifted curvatures for different damage levels for the first mode of vibration

TABLE V ACTUAL AND INFERRED FREQUENCIES FOR A RANGE OF DAMAGE LEVELS

k	Actual ω (rad s-1)	ω from optimisation (rad s-1)
50	4.9348	4.9348
49	4.8361	4.8361
48	4.7374	4.7374
47	4.6387	4.6387
46	4.5400	4.5400

The frequencies determined from the optimisation approach are an exact match of the actual frequencies,

given the number of significant digits considered here, for each of the five damage levels. While the proposed time-shifted curvatures involve second derivatives, it is clear that they show promise as a damage indicator.

VI. RESULTS OF TIME-SHIFTED CURVATURES FOR TWO MODES OF VIBRATION

A second mode of vibration is now included in simulations. The beam displacements generated in Section II for two modes of vibration are used again here. The theoretical expression for the time-shifted curvature now becomes:

$$\kappa = A_1 \sin(\omega_1 t_{r-d} + \tan^{-1}\phi_1) + A_2 \sin(\omega_2 t_{r-d} + \tan^{-1}\phi_2)$$
(26)

where A_1 and A_2 are determined from (23) for $n = 1$ and $n = 2$ respectively, φ_1 and φ_2 are determined from (24) and ω_1 and ω_2 are the two decision variables in the optimisation problem, for the frequency of the first and second mode respectively.

The optimisation approach is now used with five unknown variables; frequencies of the two modes of vibration, the difference in phase angle between the modes and the amplitudes of the two modes. Damage is included in simulations and the variables, determined from the optimisation, are given in the Table VI.

TABLE VI INFERRED FREQUENCIES, AMPLITUDES AND PHASE DIFFERENCE FOR A RANGE OF DAMAGE LEVELS

k	ω_1 (rad s-1)	ω_2 (rad s-1)	A_1	A_2	Φ Diff (rad)
50	4.9348	19.7393	1.0000	0.1000	0.7854
49	4.8361	19.3444	1.0000	0.1000	0.7854
48	4.7374	18.9497	1.0000	0.1000	0.7854
47	4.6387	18.5548	1.0000	0.1000	0.7854
46	4.5400	18.1600	1.0000	0.1000	0.7854

Fig. 11 illustrates the time-shifted curvatures determined from the bridge deflections measured by the moving vehicle for different levels of damage.
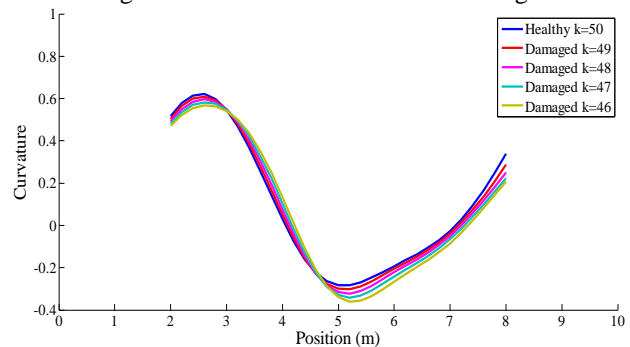

Fig. 11: Time-shifted curvatures from the moving vehicle model for different levels of damage for the first and second mode of vibration

While the inclusion of the second mode of vibration clearly changes the shape of the time-shifted curvatures, it is clear that damage is still detected successfully.

A. Implications of White Noise in Measurements

The beam displacements generated in Section II for two modes of vibration are used again here. Additive White Gaussian Noise (AWGN), according to [30] is added to the displacements before the time shifted curvatures are calculated in (27).

$$D_{Poll} = D + E_{Noise}^2 \times Noise \qquad (27)$$

where D_{Poll} is the displacement signal containing noise, D is the original displacement signal containing no noise, $Noise$ is a standard normal distribution vector with zero mean and unit standard deviation and E_{Noise}^2 is the square of the energy in the noise. The term, E_{Noise}^2, is determined from the definition of the Signal to Noise Ratio (*SNR*) given by (28).

$$SNR = 10\log_{10} \frac{\mathrm{var}\, D}{E_{Noise}^2} \qquad (28)$$

This is the ratio of the power in the signal to the power in the noise, where $\mathrm{var}D$ is the variance of the displacement signal. In these simulations, the *SNR* is specified, and $\mathrm{var}D$ is easily determined. Using (28), noise at *SNR* levels of 100, 50, 33 and 25 are added to the beam displacements and then the optimisation approach from Section VI is used with five unknown variables; frequencies of the first two modes, the difference in phase angle and the amplitudes of the two modes. Five levels of damage are included and the mean first natural frequency of 20 simulations, with error bars of ± one standard deviation, for the four noise levels can be seen in Fig. 12.
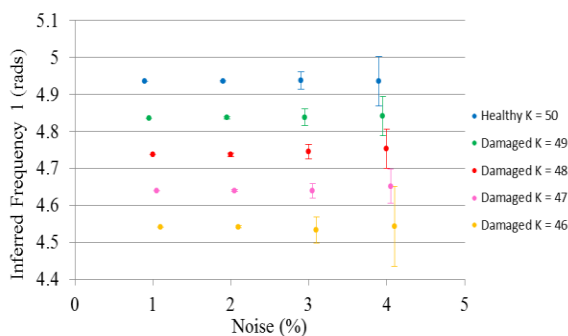

Fig. 12: Influence of noise on the ability of time-shifted curvatures to detect changes in the first natural frequency

The Fig. 12 illustrates that the approach proves insensitive to noise for levels up to an SNR value of 33.33 (3% noise).

VII.   CONCLUSIONS

This paper investigates the feasibility of using an instrumented vehicle model to detect damage in a bridge. An optimisation approach is proposed as an alternative to standard signal processing techniques because of the brevity of the signal. Time-shifted curvatures are proposed to remove contamination due to the road profile. Simulations show that modest losses of stiffness in the bridge can be detected using the vehicle measurements, even in the presence of significant noise levels. Overall the results presented in the paper indicate that the method has the potential to be developed as an effective tool for the monitoring of bridge damage.

REFERENCES

[1] S.C.W. Kim, M. Kawatani, "Challenge for a drive-by bridge inspection," *in Proc of the 10th International Conference on Structural Safety and Reliability*, 2009, p. 758–765, Osaka, Japan.

[2] A. González, E. Covián, J. Madera, "Determination of bridge natural frequencies using a moving vehicle instrumented with accelerometers and a geographical positioning system," *in Procs of the Ninth International Conference on Computational Structures Technology*, 2008, paper 281, Athens, Greece.

[3] C.W. Lin, Y.B. Yang, "Use of a passing vehicle to scan the fundamental bridge frequencies: An experimental verification," *Engineering Structures*, vol. 27, pp. 1865-1878, 2005.

[4] T. Toshinami, M. Kawatani, C.W. Kim, "Feasibility investigation for identifying bridge's fundamental frequencies from vehicle vibrations," *in Proc of the Fifth International Conference on Bridge Maintenance, Safety and Management*, 2010, p. 317-322, USA.

[5] P.J. McGetrick, C.W. Kim, A. González, E.J. OBrien, "Dynamic axle force and road profile identification using a moving vehicle," *International Journal of Architecture, Engineering and Construction*, vol. 2, pp. 1–16, 2013.

[6] W.J. Staszewski, A.N. Robertson, "Time-frequency and time-scale analyses for structural health monitoring," *in Philosophical Transactions of the Royal Society A Mathematical, Physical and Engineering Science*, vol. 365, pp. 449–477, 2007.

[7] P.J. McGetrick, A. González, E.J. OBrien, "Monitoring bridge dynamic behaviour using an instrumented two axle vehicle," *Bridge and Concrete Research in Ireland*, 2010, Cork, Ireland.

[8] E.J. OBrien, J. Keenahan, "Using Instrumented Quarter-Cars for 'Drive By' Bridge Inspection," *Assessment, Upgrading and Refurbishment of Infrastructures, International IABSE Conference*, 2013, Rotterdam, Netherlands.

[9] J. Keenahan, E.J. OBrien, P.J. McGetrick, A. "González, Using instrumented vehicles to detect damage in bridges," *15th International Conference on Experimental Mechanics*, 2012, paper 2934, Porto, Portugal.

[10] A.V. Oppenheim, A.S. Willsky, S.H. Nawab, *Signals and Systems*, 2nd Ed, Prentice-Hall, 1997.

[11] D. Pines, L. Salvino, "Structural health monitoring using empirical mode decomposition and the Hilbert phase," *Journal of Sound and Vibration*, vol. 294, pp. 97–124, 2006.

[12] N.E. Huang, S. Shen, S. Long, M. Wu, H. Shih, Q. Zheng, N. Yen, C. Tung, H. Liu, "The empirical mode decomposition

and the hilbert spectrum for nonliner and nonstationary time series analysis," *in Proc of the Royal Society of London A*, vol. 454, pp. 903–995, 1998.

[13] S. Qian, D. Chen, "Joint time-frequency analysis. Signal Processing Magazine," *IEEE*, vol. 16, 52–67, 1999.

[14] H. Kim, H. Melhem, "Damage detection of structures by wavelet analysis," *Engineering Structures*, vol. 26, 347–362, 2004.

[15] A. González, E.J. OBrien, P.J. McGetrick, "Detection of bridge dynamic parameters using an instrumented vehicle," in Proc of the Fifth World Conference on Structural Control and Monotoring, 2010, paper 34, Tokyo, Japan.

[16] J. Keenahan, E.J. OBrien, P.J. McGetrick, A. González, "The use of a dynamic truck-trailer drive-by system to monitor bridge damping," Journal of Structural Health Monitoring, vol 13(2), pp. 183-197, 2013.

[17] F. Cerda, J. Garrett, Bielak, J. Barrera, Z. Zhuang, S. Chen, M. McCann, J. Kovacevic, P. Rizzo, "Indirect structural health monitoring in bridges: scale experiments," *Bridge Maintenance, Safety, Management, Resilience and Sustainability*, 2012, pp. 346–353, Stresa, Italy.

[18] X.Q. Zhu, S.S. Law, "Wavelet-based crack identification of bridge beam from operational deflection time history," *International Journal of Solids and Structures*, vol. 43, pp. 2299–2317, 2006.

[19] V. Pakrashi, A. O'Connor, B. Basu, "A Study on the Effects of Damage Models and Wavelet Bases for Damage Identification and Calibration in Beams," *Computer-aided Civil and Infrastructure Engineering*, vol. 22, pp. 555–569, 2007.

[20] V. Pakrashi, A. O'Connor, B. Basu, "A Bridge-Vehicle Interaction based experimental investigation of damage evolution," *Structural Health Monitoring*, vol. 9, pp. 285–296, 2010.

[21] D. Hester, A. González, "A wavelet-based damage detection algorithm based on bridge acceleration response to a vehicle," *Mechanical Systems and Signal Processing*, vol. 28, pp. 145–166, 2006.

[22] A. Ayenu-Prah, N. Attoh-Okine, "Comparison study of hilbert-huang transform, fourier transform and wavelet transform in pavement profile analysis," *Vehicle System Dynamics*, vol. 47, pp. 437–456, 2009.

[23] L.W. Salvino, D.J. Pines, M. Todd, J.M. Nichols, "EMD and Instantaneous Phase Detection of Structural Damage", in Hilbert-Huang transform and its applications, World Scientific Publishing, Singapore, 2005, pp. 227–261.

[24] D. Cantero, E.J. OBrien, "Tracing the evolution of bridge natural frequencies as a vehicle traverses the bridge," *in Proc of the 11th International Conference on Vibration Problems*, 2013, Lisbon, Portugal.

[25] M. Bradley, González, A., D. Hester, "Analysis of the structural response of a moving load using empirical mode decomposition", *in Proc of the 5th International Conference on Bridge Maintenance, Safety and Management*, 2010, p. 356-363, Philadelphia, USA.

[26] N. Roveri, A. Carcaterra, "Damage detection in structures under traveling loads by Hilbert–Huang transform," *Mechanical Systems and Signal Processing*, vol. 28, pp. 128–144, 2012.

[27] P.J. McGetrick, A. González, E.J. OBrien, "Theoretical investigation of the use of a moving vehicle to identify bridge dynamic parameters," *Insight: Non-destructive Testing and Condition Monitoring*, vol. 51, pp. 433–438, 2009.

[28] International Organisation for Standardisation ISO 8608, Mechanical vibration-road surface profiles - reporting of measured data, 1995.

[29] A. González, E.J. OBrien, P.J. McGetrick, "Identification of damping in a bridge using a moving instrumented vehicle," *Journal of Sound and Vibration*, vol. 331, pp. 4115–4131, 2012.

[30] R.G. Lyons, "Understanding Digital Signal Processing", 3rd Ed, Boston, USA, Prentice-Hall, 2011, pp. 867–883.